

Jointly Optimizing Color Rendition and In-Camera Backgrounds in an RGB Virtual Production Stage

Chloe LeGendre
Netflix
clegendre@netflix.com

Lukas Lepicovsky
Scanline VFX
lukas.lepicovsky@scanlinevfx.com

Paul Debevec
Netflix
debevec@netflix.com

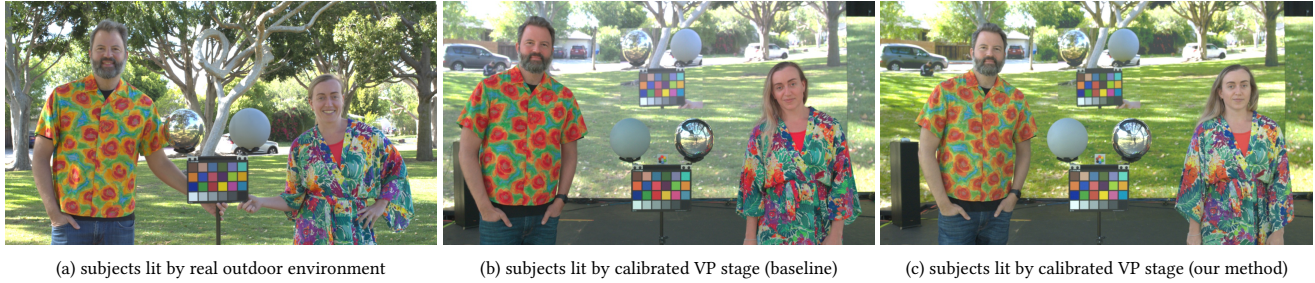


Figure 1: (a) Subjects in colorful clothing with a color chart and lighting reference spheres in an outdoor environment. (b) The same subjects in an RGB LED virtual production stage lit by color-matched imagery of the environment, showing color rendition errors in clothing colors and skin tones. (c) The subjects in an RGB LED virtual production stage calibrated using our technique to optimize both color rendition accuracy and in-camera background appearance.

ABSTRACT

While the LED panels used in today’s virtual production systems can display vibrant imagery with a wide color gamut, they produce problematic color shifts when used as lighting due to their “peaky” spectral output from narrow-band red, green, and blue LEDs. In this work, we present an improved color calibration process for virtual production stages which ameliorates this color rendition problem while also passing through accurate in-camera background colors. We do this by optimizing linear color correction transformations for 1) the LED panel pixels visible in the camera’s field of view, 2) the pixels outside the camera’s field of view illuminating the subjects, and – as a post-process – 3) the pixel values recorded by the studio camera. The result is that footage shot in an RGB LED panel virtual production stage can exhibit more accurate skin tones and costume colors while still reproducing the desired colors of the in-camera background.

CCS CONCEPTS

• Computing methodologies → Image-based rendering.

KEYWORDS

virtual production, image-based lighting, color rendition

1 INTRODUCTION AND RELATED WORK

1.0.1 Virtual Production. Although the umbrella term *Virtual Production* (VP) refers to a cadre of novel, technology-driven filmmaking methods, many recent incarnations employ LED stages to surround the actors with imagery of the virtual film locations. This technique, cast as an alternative to both filming on location and filming in a studio using a green screen, has exploded in popularity for both film and television production [Holben 2020; Kadner 2021a,c]. One benefit of filming inside a VP stage allows the actor

to be photographed against a high-resolution background image shown on the LED panels, called an *in-camera background*. This process can remove significant post-production compositing work as compared with the traditional workflows of chromakey, matting, and rotoscoping.

Beyond the in-camera background, an additional goal of filming inside an LED volume VP stage is to perform *lighting reproduction*, where an actor is surrounded from all directions by individually controllable LED units that can be driven to reproduce the illumination of a given scene [Debevec et al. 2002; Hamon et al. 2014]. When displaying a high dynamic range, image-based lighting (HDL) environment [Debevec 1998], a lighting reproduction system can generally match the subject’s appearance to how they would appear in a real environment. A further benefit is that actors may feel more immersed in the scene, potentially enhancing their performances and providing natural eyelines compared to shooting in a greenscreen studio.

1.0.2 The Unusual Spectra of RGB LEDs. Unfortunately, while RGB LED panels perform well at (and have been designed for) displaying imagery with a wide gamut of colors, they cannot reproduce any desired target illuminant *spectrum*. In particular, the emission spectra of most real-world illuminants (e.g. daylight and white LEDs, see Fig. 2) are relatively broad, covering most of the visible light wavelength range from 400 to 700 nm. In contrast, by combining different amounts of light produced by the red, green, and blue LEDs that comprise most LED display panels, one will only be able to produce illumination with relatively “peaky” emission spectra, with distinct gaps between the spectra of each LED channel (see Fig. 3). The unusual emission spectra produced by RGB LEDs leads to significant color rendition errors in typical LED volumes when comparing with color appearance under real-world illumination. It’s not sufficient for an LED panel to simply appear the same color

as the intended illuminant, since color appearance is produced by integrating the fully spectral modulation of the light source emission spectra, the camera spectral sensitivity functions, and the material reflectance spectra.

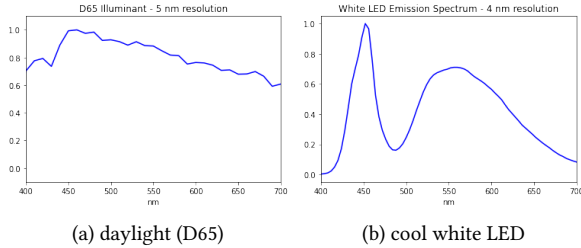


Figure 2: (a) emission spectrum of daylight (D65); (b) emission spectrum of a broad-spectrum cool white LED.

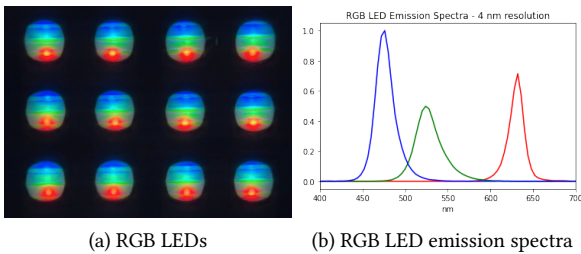


Figure 3: (a) a zoomed-in view of an LED panel showing an RGB LED package at each pixel; (b) a typical emission spectrum of an RGB LED system.

1.0.3 Color Rendition Challenges. Although LED volume VP techniques have enabled a whole new way to produce filmed content, cinematographers are becoming increasingly aware of the color rendition challenges that come with using these RGB-only systems, as recently noted and observed by Noah Kadner and Craig Kief in their recent *American Cinematographer* article “Color Fidelity in LED Volumes” [Kadner 2021b]. Most notably, in an RGB LED VP volume, skin tones shift to pink or red, orange materials shift toward red, cyan materials shift toward blue, and yellow materials darken. These color rendition errors result from the spectral gaps between the red, green, and blue LEDs, and from the relatively long wavelength of the red LEDs which illuminates skin where it is relatively more reflective. For an example, see Fig. 4. To quote sec. 3.3.3.1 of Weidlich et al. [2021], “The lack of amber spectral contribution produces a poor [color] rendition of human skin and orange objects lit by the LED wall.” Even before the rise of LED volume filming techniques, The Academy of Motion Pictures Arts and Sciences convened a “Solid State Lighting” working group in part to combat the “chromatic chaos” of solid-state illumination, culminating in the proposal of the Spectral Similarity Index (SSI) to alert cinematographers to potential color rendition challenges when using a particular light source on set [Holm et al. 2016].

1.0.4 Filling in Spectral Gaps. The color rendition impact of the spectral discrepancy between broad-spectrum, real-world light sources and RGB LED produced illumination has previously been

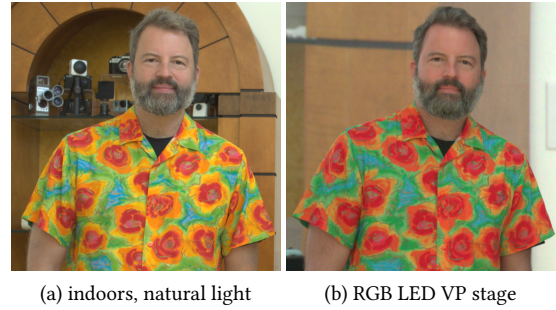


Figure 4: (a) a subject illuminated by indoor daytime natural lighting; (b) reproducing the illumination inside an RGB LED VP stage, with noticeable color rendition errors for skin tones and yellow and orange patches on the subject’s shirt.

systematically studied and quantified both for individual light sources in Wenger et al. [2003] and for omnidirectional lighting reproduction systems in LeGendre et al. [2017; 2016]. These works further demonstrated that adding spectral channels beyond RGB for solid state lighting reproduction systems can dramatically improve their color rendition capabilities. While cinema light source manufacturers now incorporate these additional spectral channels beyond RGB in their light sources (e.g. by adding a broad-spectrum white LED) to improve color rendition, there are essentially no manufactured LED panels that follow suit. LED panels have historically been manufactured to display a color gamut as wide as possible, a goal for which adding a broad-spectrum white or amber LED is unnecessary, as their colors (though not their spectra) can be matched well by RGB LEDs.

1.0.5 LED Panel Calibration Workflows. Making do without additional spectral channels, color scientists and digital imaging technologists working to color calibrate the typical RGB LED panels used in VP stages today aim to make color values in the content to be displayed actually appear those colors to the camera. This calibration process takes into account both the spectral sensitivity of the motion picture camera and the emission spectra of the RGB LEDs, although it typically requires no spectral measurements. One way of ensuring that each color displayed by the LED panel and then observed by the camera matches the target color of the content is to ensure that the pure red, pure green, and pure blue primaries all match as well. That is to say: red being displayed by the LED wall and recorded by the camera matches the target red of the content, and the same holds for green and blue. In practice this is achieved by photographing with the motion picture camera a patch of each color primary as displayed by the panels. As noted in Debevec et al. [2002], if the primaries match, then all other colors including white must match as well, as all others are simply a linear combination of the three primaries. This primary-based calibration process has been outlined by Unreal Engine (a technology provider for real-time, in-camera visual effects) in the online guide “In-Camera VFX Camera Color Calibration” [unr [n.d.]]. A variant was also introduced by VFX company Weta Digital in Thomas Mansencal’s course notes for “Applied Spectral Knowledge in Virtual Production” (see sec. 3.3.3.1 of Weidlich et al. [2021]). Both of these approaches rely on computing a color transform (usually a 3×3 color matrix to apply

to input RGB pixel values in the content to be displayed), with the goal of making the primaries of the panel-displayed content appear the correct colors to the motion picture camera.

The above primary-based calibration process is ideal when the goal is simply to use the LED panels as a display system, say, for filming an in-camera background. Difficulties arise, however, when we consider that LED panels in VP are also being used for lighting reproduction where the aforementioned color rendition challenges arise. In this case, we are no longer simply recording the appearance of the LED panels displaying content directly, but now we must consider how these panels *illuminate* actors and their costumes.

1.0.6 Using a Calibrated RGB LED Panel as a Light Source. As an example, say that we take an outdoor photograph of a color chart calibration target lit by daylight (see Fig. 5a), and we capture a high dynamic range panorama to use for IBL-based lighting reproduction in our VP stage with the same camera. From the white square of the color chart, we can extract an RGB pixel value w that represents the average color of the scene’s illumination (specifically, for the hemisphere of lighting directions facing the color chart). We know that if we practice the above LED panel calibration technique, that a color chart placed in an ideal calibrated RGB LED VP stage displaying the HDR IBL, as recorded by our motion picture camera, will have a white square value that matches w (see Fig. 5b). However, the *spectrum* of illumination falling on the chart in the VP stage is quite different from that in the real-world outdoors, and so any non spectrally flat / non-neutral squares of the color chart are unlikely to match the image of the chart captured outdoors. The comparison visualization between the charts in Fig. 5c demonstrates this effect. Note that a virtual color chart *displayed* by the panels would appear largely correct; it is only the real color chart *lit* by the LED panels inside the VP stage with will exhibit color rendition errors.

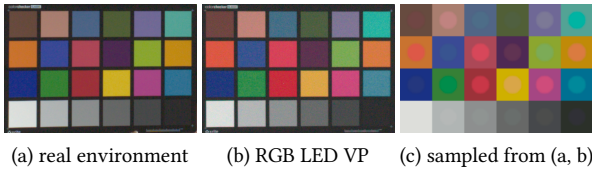


Figure 5: (a) a color chart photographed in a real outdoor environment; (b) photographed in a VP stage reproducing the target illumination using RGB LEDs and a standard primary-based calibration process; (c) comparison between (a) and (b). Background squares are pixel values sampled from (a) and foreground circles are pixel values sampled from (b). Although the white squares match (the illuminants are *metameric matches*), the remaining color squares do not.

1.0.7 Metameric Illuminant Matching. In the lighting reproduction literature, the above primary-based calibration process is termed *metameric illuminant matching* (MIM) by Wenger et al. [2003], because it guarantees that the color of the real illumination matches the color of the reproduction of the illumination. (Metamerism is defined as the perceived matching of colors with different, non-matching spectral power distributions.) Both Wenger et al. [2003]

and LeGendre et al. [2016] presented the limitations of color rendition when attempting to replicate real-world illuminants using only RGB LEDs with MIM.

1.0.8 Our Approach. While these previous works suggested to overcome such color rendition challenges by adding further spectral channels to the light sources used for lighting reproduction, in this present work we present an alternative solution that improves color rendition while using only the RGB LEDs currently available in most LED volume VP stages. Specifically, we propose a novel technique for the color calibration of an LED volume stage using a *set* of linear transformations represented as 3×3 color correction matrices. Our goal is to optimize the color rendition properties of the LED volume acting as a light source, while also achieving accurate in-camera panel appearance. Since we know that RGB LEDs produce color rendition errors when simulating broad-spectrum lighting, we propose, in contrast to prior work, to solve for an optimal post-correction matrix to improve color matching. Such a post-correction matrix can desaturate overly pink/red skin tones while keeping neutral colors neutral, which cannot be accomplished by altering the content displayed on the LED stage alone. We further show that if we apply the inverse of the post-matrix to the in-camera-frustum area, then the in-camera panel appearance can be matched as well, similar to primary-based, MIM calibration techniques currently practiced in production.

In our technique, we thus employ three different matrices, as shown in Fig. 6:

- (1) a 3×3 pre-correction matrix M to be applied to the pixel values of the LED displayed content for the out-of-camera-frustum pixels (the parts of the LED stage predominantly used for illumination, not visible in-camera);
- (2) a different 3×3 pre-correction matrix N to be applied to pixel values of the LED displayed content, for the in-camera-frustum pixels (which appear as the in-camera background);
- (3) and a third 3×3 post-correction matrix Q to be applied to the final imagery captured by the camera, which color corrects both the in-camera background and recorded foreground content together, without requiring any foreground/background separation.

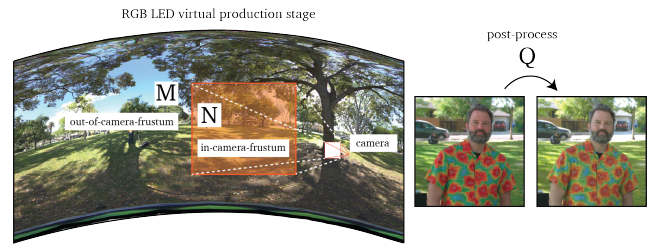


Figure 6: A visualization of our method. A 3×3 pre-correction matrix M is applied for out-of-frustum content, while a different 3×3 pre-correction matrix N is applied for in-camera-frustum content. Finally, a 3×3 post-correction matrix Q is applied to the recorded image content.

As described, previous approaches for LED panel color calibration have concentrated on the in-camera background imagery (using only one 3×3 matrix or color transform), while not considering

the color rendition properties of the resulting illumination falling on the actors, and have not considered an adaptive post-correction strategy. Our approach, in contrast, ensures near optimal color rendition simultaneously both for foreground content (e.g. actors, set, costumes) as well as the in-camera background content where LED pixels are observed directly. Our technique requires no spectral measurements of any part of the system (camera, materials, or LED panels), relying only on four images captured with the principal-photography camera for a given LED volume. While two of the three matrices that we propose will be unique to each target lighting environment, the calibration images used to compute these optimal matrices need only to be captured once for each camera/LED volume combination.

2 METHOD

We begin with a high-level overview of our approach. Then, in the remainder of this section, we present the prerequisites and assumptions that we make about our full imaging pipeline, followed by the calibration images required to practice the proposed technique. Throughout, we justify our approach.

2.1 Overview

In summary, our full process can be described by the following straightforward steps:

- (1) We solve for a 3×3 matrix \mathbf{M} that maps the target scene’s pixel colors to the LED panel colors, so they look the same to the motion picture camera. In general, applying \mathbf{M} to the displayed content will not, however, *light* the stage subjects accurately, as colors will appear overly-saturated.
- (2) We thus solve for 3×3 *post-correction* matrix \mathbf{Q} that will make a photographed color chart lit by the VP stage displaying the HDR IBL environment look as close as possible to how it appeared in the real scene. However, if we apply \mathbf{Q} to the whole image, the in-camera background pixels will no longer appear correct.
- (3) Thus, instead of applying \mathbf{M} to the in-camera-frustum pixels, we apply a different 3×3 matrix $\mathbf{N} = \mathbf{M}\mathbf{Q}^{-1}$. As the background pixels do not contribute significantly to the lighting on the actors, both the color rendition on the actors and the appearance of the in-camera pixels are optimized.

2.2 Assumptions and Prerequisites

2.2.1 Panel and Camera Linearity. Our method first assumes that an LED volume has been calibrated to act as a linear display. This means that if you ask it to display a given pixel value p and it generates lighting spectrum l in some radiometric units, then asking it to display the pixel value ap results in the panel generating a proportional light spectrum al , as long as ap does not exceed the maximum brightness of any of the panel’s channels, and ignoring quantization. Images of displayed color swatch ramps, or an image series shot with increasing pixel values on the LEDs [Debevec et al. 2002] can be used to verify linearity, and if needed, to correct it.

Our method also assumes that the camera used throughout the imaging workflow also has a linear response, as it is typical for digital cinema or even “prosumer” cameras to output linear data through RAW (or at least linear) file formats. In this work, we

verified the LED panels showed images with a gamma value of 2.4, and gamma-corrected all linearly computed images for display accordingly.

2.2.2 Radiometric Alignment of Different Panel Types. LED volumes in practice are often comprised of multiple types of LED panels, depending on whether they are designed to cover a studio’s ceiling, wall, or floor. Our method also further assumes that the relative brightness levels of different panel types comprising an LED volume have been calibrated such that a pixel value of $[1, 1, 1]$ displayed from all directions produces as uniform as possible of a sphere of light of even intensity and color balance from all directions. For example, if a ceiling LED panel with a larger pixel pitch has the ability to generate more total illumination than a wall or floor LED panel, the ceiling panel should be radiometrically adjusted to match the light output of the wall. As another example, if a ceiling panel’s white point displaying $[1, 1, 1]$ is more “blue” than the wall or floor LED panels, its white balance should first be adjusted to match the color output of the wall. This step also falls within the standard practice for LED volume calibration.

2.2.3 HDRI Map Acquisition and Display. We assume that the lighting environment to be displayed on the VP stage will be captured using high dynamic range, panoramic photography techniques (e.g. [Debevec 1998]). We further assume that a color chart has been photographed at a spatial location such that the HDR panorama’s center of projection matches the location of the color chart in the scene. In practice, this means that our technique could be less accurate for color charts shot at some distance from the HDRI map’s location. Finally, we assume that the VP stage is capable of representing the full dynamic range of the HDRI map, without clipping any light sources.

2.3 Calibration Images and Equations

Our technique requires the capture of just four calibration images, all photographed using the target motion picture camera that will be used for filming in the LED volume. We next describe these photographs, providing intuition as to why they are needed. The first is of the LED panels displaying color patches for each primary color, required for computing \mathbf{M} . The second, third, and fourth images record how each spectral channel of the LED stage *lights* a color calibration target, required for computing \mathbf{Q} .

2.3.1 Solving for \mathbf{M} : Primary-based Calibration for Metameric Illuminant Matching. This measurement allows us to map the target scene’s pixel colors to LED panel colors observed by the motion picture camera, ensuring a metameric illuminant match when a scene’s HDRI map is displayed. For this calibration, we display a patch of pure red, pure green, and pure blue on the in-camera-frustum LED panels and record their appearance to the camera, directly measuring the appearance of each LED channel in the VP stage to the camera (see Fig. 7). These patches can all be photographed in a single image.

This is the same process that is used to generate a primary-calibrated LED panel [unr [n.d.]; Weidlich et al. 2021] or metameric illuminant match as in Wenger et al. [2003]. From these images, we extract average pixel values for a region of interest, corresponding to how the camera observes pure red, green, and blue displayed



Figure 7: Square patches of red, green, and blue LEDs as observed by our motion picture camera. These are shown in camera raw before any color calibration. Pixel values sampled from these images form the $[SL]$ matrix, which encodes how the camera observes the LED primaries.

by the LED panels. We concatenate these sampled values along columns to obtain a 3×3 matrix that we call $[SL]$, because its elements are the pairwise dot products of the camera’s Spectral sensitivity functions and the LED emission spectra. $[SL]$ has the camera’s color channels along rows, and the spectral channels of the LED volume along columns. We ensure that out-of-frustum panels are turned off during this capture, to prevent including light bounced off the front side of the panels in the measurement.

From $[SL]$, we can directly solve for our 3×3 metameric illuminant matching matrix M given the equation:

$$[SL]MI = I \quad (1)$$

In this equation, I represents the identity matrix. This equation holds because our goal is that pixel values corresponding to pure red, green, and blue ($[1, 0, 0]$, $[0, 1, 0]$ and $[0, 0, 1]$) displayed by the panel are observed as the same pixel values to the camera. We can also think of this equation as linearly combining the LED primaries as seen by the camera (columns of $[SL]$) to produce the final pixel values of our image. We can easily solve for M using matrix inversion:

$$M = [SL]^{-1} \quad (2)$$

Thus far, this process is nearly identical to that used for calibrating a typical VP stage for in-camera VFX. However, in our technique we will use M as a color correction matrix for out-of-frustum content only, rather than for all content as before.

2.3.2 Solving for post-correcting Q : Color Rendition Calibration. Next, our goal is to solve for a 3×3 *post-correction* matrix Q which, when applied to the final image, makes a color chart lit by the VP stage displaying the HDR IBL environment look as close as possible to how it appeared in the real scene. It is common practice to capture a slate including a color calibration target such as the X-Rite ColorChecker Chart during filming, so we anticipate that such a test target will be available. While we could, in practice, just photograph the chart as illuminated by the HDR IBL displayed by the panels (pre-corrected with M), and solve for Q from this image directly, ideally we would be able to compute Q only from calibration imagery, captured once regardless of the number of lighting environments that we wish to display.

Towards this end, we photograph calibration imagery of the color chart as illuminated by each channel of the LED volume (the red, green, and blue spectral channels individually), following the

procedure outlined by LeGendre et al. [2016]. The core insight here is that because of the superposition principle for light, any chart illuminated by the VP stage will resemble a linear combination of these three images. So, if we capture such data, we can simulate the appearance of a color chart illuminated by any given environment, rather than needing to photograph it each time to compute Q .

To capture these photographs, we turn on a $1m \times 1m$ square of the LED wall for each spectral channel, and we place our color chart 1m from the center of the square aimed directly toward the LED wall. We orient our camera such that its optical axis makes a 45° angle with the surface normal direction of the color chart, leveraging the property that the color chart reflects light diffusely. We show this setup in Fig. 8 (top row), and the resulting calibration images captured for our camera in Fig. 8 (middle row), and, finally, the pixel values sampled from these images in Fig. 8 (bottom row).

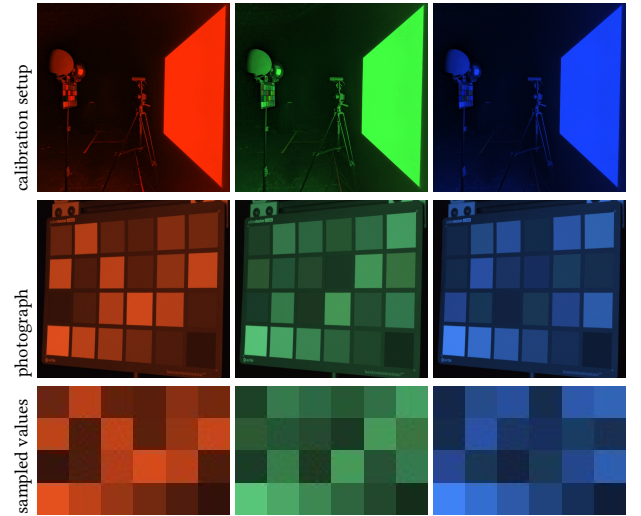


Figure 8: Top row: our color rendition calibration setup, photographed with a witness camera. A color chart is placed in front of a $1m \times 1m$ square of illuminated LED panel, with the chart parallel to the panel surface. The motion picture camera is placed 45° off-angle from the surface normal of the chart. Middle row: photographs of the color chart lit by each spectral channel. Bottom row: pixel values sampled from the images of the middle row.

Although we know that the pixel values sampled from a color chart illuminated by any HDR IBL environment displayed in the VP stage and observed by our camera must be a linear combination of the sampled pixel values of our calibration data in Fig. 8 (bottom row), we must determine for a specific environment *how much of each image* to add together to simulate a color chart’s appearance. For this, we first need to know the relationship between amount of light represented by the $1m \times 1m$ square of light as compared with the full sphere of illumination (assuming an ideal virtual production stage with no missing lighting directions). We further need to know how much of each spectral channel will be used when displaying each unique lighting environment in the VP stage.

We first define a scale factor β that accounts for the fact that the $1m \times 1m$ square of illumination, placed 1m away from the

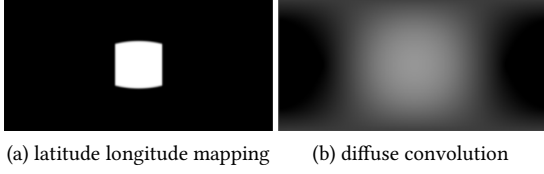


Figure 9: (a) A latitude-longitude mapping of the calibration setup: a $1\text{m} \times 1\text{m}$ panel viewed from a 1m distance; (b) The diffuse convolution of (a). From (b) we solve for the scale factor β that adjusts for the intensity difference between our calibration setup and a full, even sphere of illumination.

color chart, represents a smaller solid angle compared with the full sphere of illumination. We construct a cube map environment with a square representing the panel. Our setup geometry suggests a ~ 54 pixel width square for a cube map with a face width of 90 pixels, representing $\sim 54^\circ$. We convert this cube map to a latitude-longitude mapping (see Fig. 9), which yields $\beta \approx 0.311$ for a the 1m square at a 1m distance. Thus, our calibration images should be scaled by $\frac{1}{\beta}$. This scale factor depends only on the setup geometry, and not the individual type of LED panel or camera used. In general, as real-world VP stages will be missing some lighting directions and may not contain emissive flooring, this technique is designed to require only a $1\text{m} \times 1\text{m}$ square of LED panels plus a scale factor, rather than omnidirectional, even illumination. Nonetheless, using this technique, we are able to predict how a color chart would appear when lit with uniform, omnidirectional illumination for each spectral channel.

To determine how much of each spectral channel will be used when displaying a *particular* lighting environment in the VP stage, we leverage the fact that a color chart reflects light mostly diffusely according to Lambert’s law, integrating its full frontal hemisphere of lighting directions. Thus, for the purposes of color rendition, we only care about the diffuse integral of the illumination in the VP stage, rather than the individual contributions of each pixel in the LED panels. We define the diffuse integral of the frontal hemisphere of the HDRI map as the RGB pixel value \mathbf{w}_{avg} . If the target color chart is photographed while placed at center of projection of the HDRI panorama, then \mathbf{w}_{avg} is equal to the pixel value of the white square of this color chart, scaled up to adjust for the fact that the white square of a typical color chart is only $\sim 90\%$ reflective. Thus, instead of simply summing together images of the color chart as illuminated by a full sphere of illumination for each spectral channel, we can now scale these images based on the expected overall diffuse integral for a given lighting environment, expressed as \mathbf{w}_{avg} . This is essentially *tinting* the full, even sphere of illumination based on the white balance of the given environment, which can be measured directly from the appearance of the white square of a color chart placed in the original, real-world scene. However, we are employing the pre-correction matrix \mathbf{M} when displaying the out-of-frustum content responsible for color rendition. Thus, rather than tinting the full, even sphere of illumination using \mathbf{w}_{avg} , we must instead tint it using $\mathbf{M}\mathbf{w}_{\text{avg}}$.

Formally, with the above calibration data, we can now estimate how a color chart illuminated by the VP stage displaying a particular

HDR IBL will appear, which we will finally use to solve for \mathbf{Q} . For a given color chart square j , we define a 3×3 matrix $[\mathbf{SRL}]_j$ that encodes the fully-spectral modulation and integration of the camera spectral sensitivity functions, the LED emission spectra, and the material reflectance spectrum. As with the previously defined $[\mathbf{SL}]$ matrix, $[\mathbf{SRL}]_j$ has the camera’s color channels along rows, and the spectral channels of the LED volume along columns. In other words: each column encodes the RGB pixel values of how a particular color chart square j appears when illuminated by each available spectral channel in the VP stage. Note that there will be a different $[\mathbf{SRL}]$ matrix for each chart square, as each square has a unique reflectance spectrum. The pixel values for each $[\mathbf{SRL}]$ matrix are captured by our calibration process, represented by the sampled values in Fig. 8 (bottom row). Finally, the expression to predict how a given chart square j will appear when illuminated by the VP stage displaying an HDR IBL with diffuse integral \mathbf{w}_{avg} and out-of-frustum matrix \mathbf{M} is:

$$\frac{1}{\beta} [\mathbf{SRL}]_j \mathbf{M} \mathbf{w}_{\text{avg}}. \quad (3)$$

Our ultimate goal is to match the color rendition properties of the original scene, with target color chart values \mathbf{p} . Thus, including the desired post-correction matrix \mathbf{Q} , we would like to minimize the squared error between the predicted pixel values and the target pixel values across all n chart squares:

$$\arg \min \left(\sum_{j=1}^n \left\| \frac{1}{\beta} \mathbf{Q} [\mathbf{SRL}]_j \mathbf{M} \mathbf{w}_{\text{avg}} - \mathbf{p}_j \right\|^2 \right). \quad (4)$$

Each chart square yields three equations (one each for the red, green, and blue channels of the final image), while \mathbf{Q} contains nine unknown variables. We could therefore choose three chart squares to match exactly, or we could use all 24 squares of the color chart to solve for \mathbf{Q} in a least squares sense. Recall, in Eqn. 4, $[\mathbf{SRL}]$ values are obtained from calibration imagery, while \mathbf{w}_{avg} and \mathbf{p} are sampled from the target color chart in the original environment. \mathbf{M} was computed using the primary-calibration procedure. Thus, while \mathbf{M} is lighting environment independent, \mathbf{Q} depends on the appearance of a color chart in a particular environment and thus will change depending on the target HDRI map.

2.3.3 Solving for \mathbf{N} : Inverting the effect of \mathbf{Q} for the in-camera background. Unfortunately, if we apply the 3×3 post-correction matrix \mathbf{Q} to the whole image, the in-camera background pixels will also be transformed and may no longer appear correct. While foreground detection or rotoscoping could allow the correction to be applied only to the foreground, this would require additional complexity. Our key insight here is that if we know in advance the post-correction matrix \mathbf{Q} that we will ultimately apply to the final image or video sequence, we can apply the inverse of this correction to the in-frustum part of the LED panels with \mathbf{Q}^{-1} . As the background pixels do not contribute to the lighting on the actors significantly, both the color rendition on the actors and the appearance of the in-camera pixels can be optimized at the same time, with no foreground/background separation required.

Given \mathbf{Q} and \mathbf{SL} , we can rewrite Eqn. 1 now to solve for a new in-camera-frustum pre-correction matrix \mathbf{N} :



Figure 10: LDR images of the spectrally-diverse HDR lighting environments that we reproduced in our experiments.

$$\mathbf{Q}[\mathbf{SL}]\mathbf{N}\mathbf{I} = \mathbf{I}. \quad (5)$$

Thus we can solve for \mathbf{N} :

$$\mathbf{N} = [\mathbf{SL}]^{-1}\mathbf{Q}^{-1}. \quad (6)$$

Furthermore, we can also substitute \mathbf{M} for $[\mathbf{SL}]^{-1}$, clarifying the relationship between the in-camera-frustum and out-of-camera-frustum matrices:

$$\mathbf{N} = \mathbf{M}\mathbf{Q}^{-1}. \quad (7)$$

In summary, we pre-correct the in-frustum content with \mathbf{N} , expecting to post-correct the content with \mathbf{Q} . As \mathbf{Q} is lighting environment dependent, \mathbf{N} will also vary based on the target HDRI map. In practice, since \mathbf{Q} will typically desaturate pixel colors, \mathbf{Q}^{-1} will typically increase the saturation of pixel colors. Because of this, it is recommended to ensure that the LED panels are set to display in their widest possible color gamut, consisting of primaries which turn on each LED spectrum independent of the others.

2.4 Black Level Subtraction

A current limitation of LED panels used for in-camera backgrounds is that the panels themselves reflect back some of the light which hits them, i.e., they have a non-zero *albedo*. This means that the panels oriented to light the actors also have the unwanted side-effect of illuminating the panels used for displaying the in-camera background. In our experiments, we observed panel albedos varying from ~ 4 -10%. To compensate for this, we adjust the pixel values displayed within the camera frustum with an RGB offset, computed based on a "black level" measurement. For each lighting environment, we turn on all the out-of-frustum content, first applying \mathbf{M} . Next, we turn off the in-camera background, and record with our camera a per-lighting-environment average RGB color to subtract from the rendered content prior to display. In practice, we sample a region of interest from such an image, which yields the RGB pixel value b_{camera} . This pixel value cannot be used directly for the black level subtraction for the content, as we need to factor in the scale factor between the rendered content and its camera-observed value. We can sum together the calibration images of Fig. 7 to obtain a pixel value w_{camera} of the camera observing a pixel value of $[1, 1, 1]$. The black level we subtract from the final rendered content is thus computed as $\frac{b_{\text{camera}}}{w_{\text{camera}}}$. The downside of this approach is that it requires per-lighting-environment empirical measurement. Future work could aim to analytically estimate the black level subtraction via light transport, given w_{camera} , measured panel albedo, and the HDRI map, or to measure the radiosity form factors within the stage directly using a wide-angle camera and a discretized lighting basis.

3 RESULTS

In this section, we present experimental and theoretical results of our full method, evaluating the technique when reproducing the color rendition properties of several real-world lighting environments.

3.0.1 HDR Lighting Environment Measurement and Real-World Photography. For our experiments, we captured seven spectrally-diverse lighting environments using a Canon 5D Mark III and a Canon 8-15mm fisheye lens with a 180° field-of-view, using multiple exposure HDR photography. Five of these lighting environments were captured indoors in a living room environment, each with its own distinct type of illumination: (1) broad-spectrum warm white LED lighting, (2) incandescent (tungsten halogen) lighting, (3) daylight shining through windows, (4) RGB LED "white" light, and (5) monochromatic yellow-orange sodium vapor lighting, with a distinct emission spectrum spike at 589 nm. The remaining two lighting environments were captured outdoors at a local park, (6) in the shade and (7) in direct sunlight. We show LDR renderings of the lighting environments in Fig. 10. With the camera outfitted with the fisheye lens, and using a nodal tripod mount, we captured an HDR series facing in four directions in the scene, spaced 90° apart. We were careful that no light sources clipped at each shortest exposure, with the exception of the sun, whose missing energy we reconstructed using the appearance of the white square of a color chart placed in the scene leveraging prior techniques [Debevec 2003]. We calibrated an aperture-dependent radial lens fall-off, appropriately scaling the merged HDR images before stitching the different views together to assemble each lighting environment into an 8k panorama using PTGui [PTG [n.d.]].

In each environment, to capture the color rendition properties of the real-world illumination, we additionally photographed two subjects wearing brightly colored patterned clothing, along with a color chart, a diffuse gray sphere, and a mirrored sphere as reference. For these images, we ensured that the panorama's center of projection was located near the placement of the color chart in the scene. For these reference photographs, we used the same camera outfitted with a 40mm lens and an HDR exposure series matching that of the panorama capture.

3.0.2 Lighting Reproduction in an RGB VP Stage. To test our technique, we reproduced each lighting environment inside a cylinder-shaped RGB LED based virtual production stage including floor, ceiling, and wall LED panels. Although the stage did not produce a full 360° of illumination, we ensured a setup that maximized coverage of frontal lighting directions while still allowing us to record an in-camera background. With a lux-meter, we measured the relative amount of light output by the panels for input linear pixel values ranging from 0 to 1 in step sizes of 0.25, ensuring system linearity. Inside the VP stage, we captured all images using a ZCam E2 compact cinema camera outfitted with a Laowa 17mm MFT

lens. Our spherical content was displayed the LED panels using the Unreal Engine, with camera tracking to adjust the camera frustum in real-time. Within Unreal, we added a color matrix operation to the in-frustum and out-of-frustum shaders separately to implement our approach.

To evaluate the effect of \mathbf{Q} and \mathbf{N} on the in-camera background displayed colors, we composited the color charts photographed in the real environments into the HDRI maps, careful to match the exposures, such that they would appear behind our actors when displaying the HDRI maps. As our main focus was color rendition, we did not try to match the perspective of the virtual camera with our real world camera, so the in-camera backgrounds in our experimental results are not precisely aligned with those of the real-world imagery. The backgrounds displayed in the VP stage are from the HDRI map, shot from the perspective of the subjects rather than from that of the camera used for our reference portraits.

In general, real-world light sources will be orders of magnitude brighter than the rest of a scene. However, in practice, VP stages have a limited dynamic range. To achieve a sufficiently bright in-camera background appearance for the composited color charts, we required a white square pixel value greater than 0.1. With this scale constraint, the maximum pixel values of the HDRI maps ranged from 40 to 3000 (allowing sun energy to spread to more than one pixel), well beyond the maximum panel-displayable value of 1. To prevent light source clipping in the VP stage, prior to displaying the content we used an energy-preserving light source dilation algorithm [Debevec and LeGendre 2022] for each HDRI map.

3.0.3 Experimental Results. Throughout this results section, we use one consistent color matrix to take all images from a camera raw color space to sRGB for display as a post-process for the purpose of visualization. This matrix was computed from a color chart photographed in a daylight scene using the Canon 5D Mark III. When we report quantitative error metrics, these measurements, however, are computed in camera raw color space.

Throughout this section, we use a color chart with inset circles as in Fig. 5, where the background squares represent pixel values sampled from a color chart photographed in a real-world lighting environment, and the foreground circles represent pixel values sampled from a chart reproduced inside the VP stage. We will sample these chart values both from a color chart *illuminated* by out-of-frustum content and one *displayed* on the LED panels in-frustum and observed directly by the motion picture camera. For these visualizations, we scale the sampled pixel values such that the green channel of the white squares match to facilitate visual comparisons. In practice, our VP stage is missing some lighting directions, so the out-of-frustum lit chart is typically dimmer than the in-frustum displayed chart.

In Fig. 11, we show images demonstrating our full process including intermediate results for the outdoors, shaded environment. As compared with the real photograph captured outdoors [column (a)], reproducing the illumination in the VP stage using the baseline primary-based/MIM calibration approach leads to the expected overly saturated skin tones and reddish hue shift for yellow and orange materials [column (b)]. Applying the post-correction matrix \mathbf{Q} [column (c)] desaturates these colors, improving color rendition, as observed for the comparison charts, skin tones, and clothing.

However, \mathbf{Q} also adds a blueish tint to the in-camera *displayed* chart, visible in the comparison chart of column (c). Applying $\mathbf{N} = \mathbf{M}\mathbf{Q}^{-1}$ to the in-frustum content removes this blueish tint [column (d)], but color rendition is still poor for the in-camera background due to the non-zero panel albedo and bounced light. Our black level subtraction for the in-frustum content [column (e)] thus provides the most dramatic improvement for the in-camera background. While small mismatches remain, we achieved our target goal of desaturating skin tones and improving orange/yellow material color rendition, without sacrificing the in-camera background colors. Unfortunately, the VP stage lacked light sources for the lighting directions corresponding to those providing the rim lighting on the subject’s left side of the face, somewhat limiting the quality of the overall reproduced illumination.

For the remaining six environments, we show the real-world photographs, then the baseline VP lighting reproduction using \mathbf{M} only for both in- and out-of-frustum content, and then our full multi-matrix pipeline with black level subtraction in Fig. 12 and Fig. 13. For the most part, the *lit* color chart in the VP stage is overly saturated, with hue shifts in yellow and orange materials using the baseline calibration approach with \mathbf{M} only, with the exception of the RGB LED based white lighting environment. We anticipated this result, as the RGB LEDs of the VP stage are quite good at reproducing the illumination of an RGB LED based lighting environment. Indeed, for the RGB LED scene, the post-correction \mathbf{Q} matrix is close to the identity and does not have a very significant effect.

However, there are color rendition challenges for the remaining scenes that include broader spectrum illumination sources. For the remaining scenes, the \mathbf{Q} matrix is able to desaturate colors as required, leading to improved color rendition for the *lit* chart. While \mathbf{Q} desaturates the overall image content, the in-frustum matrix \mathbf{N} ensures that the in-camera background content is still as close as possible to the target color appearance. However, as in Fig. 11, the black level subtraction is the more significant effect for the in-camera background color rendition due to the in-camera-frustum panels reflecting illumination from the out-of-frustum panels.

In the most extreme case, in Fig. 13 (upper row), we show that the RGB LEDs are not *at all* able to reproduce the narrow-band illumination of the sodium vapor illumination environment. The result is that while under the real-world sodium vapor lighting, materials appear nearly monochromatic (tinted yellow-orange), under the RGB-reproduced illumination they still have discernible colors. The post-correction matrix \mathbf{Q} desaturates these colors completely, satisfyingly reproducing the monochromatic look of the original scene. However, the post-correction matrix does not allow us to fully simulate the real-world narrow-band illumination of the sodium vapor lamp, as a 3×3 matrix can only help so much. There is a noticeable difference between the subjects’ clothing in the real-world scene compared with in the VP stage, even after applying \mathbf{Q} : the yellow regions of the clothing remain too dark. For the sodium vapor environment, we were not, in fact, able to solve for \mathbf{N} , because \mathbf{Q} is ill-conditioned due to the monochromatic nature of the illumination and thus \mathbf{Q}^{-1} is poorly defined. Thus, for Fig. 13 (upper row), our full technique includes only \mathbf{M} , \mathbf{Q} , and the black level subtraction.

Unexpectedly, we observed some remaining differences in the white balance of the *lit* color charts and the *displayed* color charts,

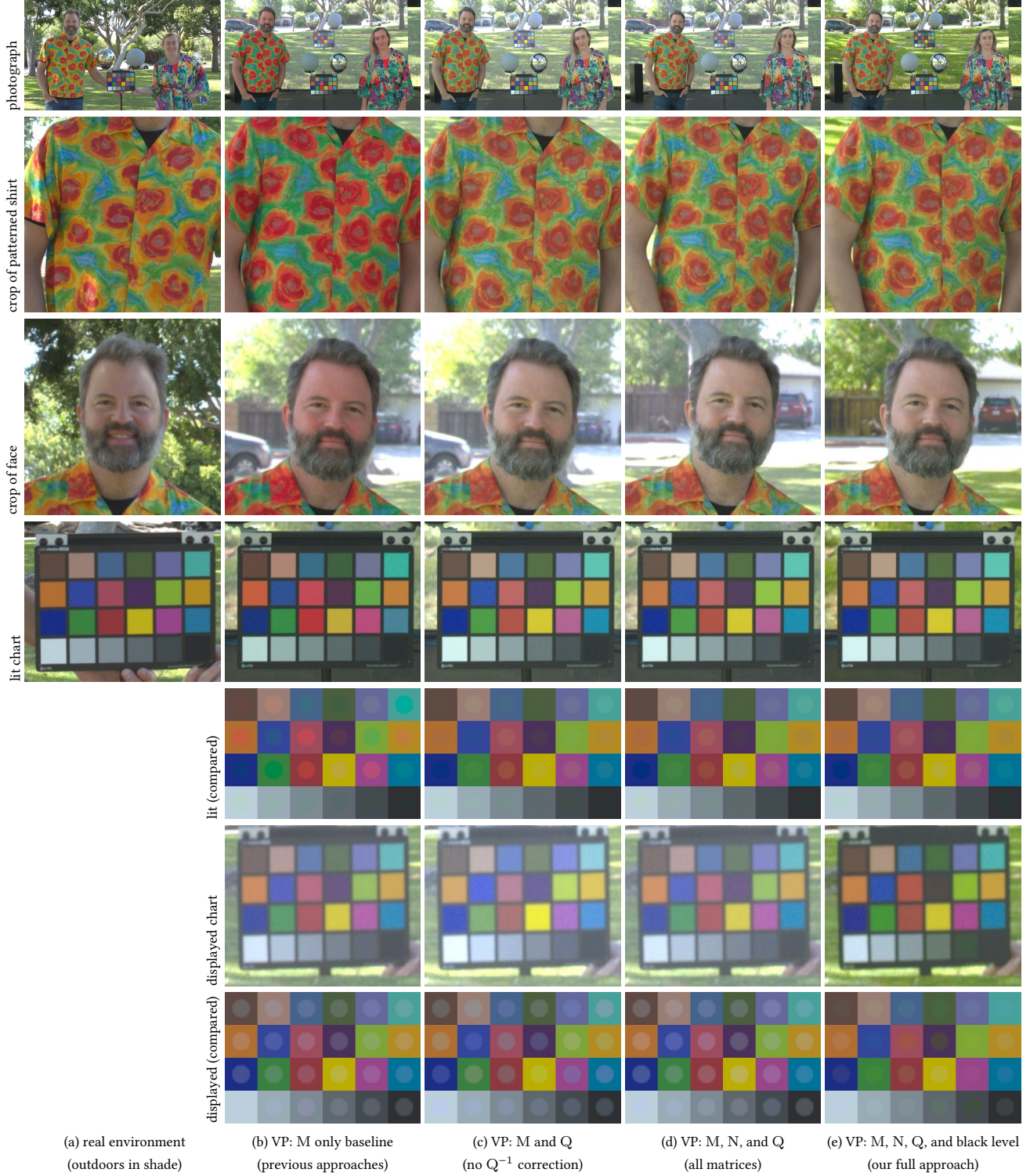


Figure 11: Column (a): two subjects photographed outdoors [Fig. 10(6)] and select crops. Column (b): VP lighting reproduction using the baseline approach (M only). Column (c): applying post-correction Q to the images of column (b). Column (d): also pre-correcting in-frustum content with N. Column (e): adding our black level subtraction. For *comparison* charts, background squares are sampled from the chart in the real environment, while foreground circles are sampled from corresponding charts in each column. In the VP stage we photographed both a chart *lit* by out-of-frustum content and *displayed* on the panels. Compared with the baseline (b), Q enables improved color rendition for the *lit* chart, desaturating skin tones and improving the appearance of orange/yellow materials. Black level subtraction provides a dramatic improvement to *displayed* content.

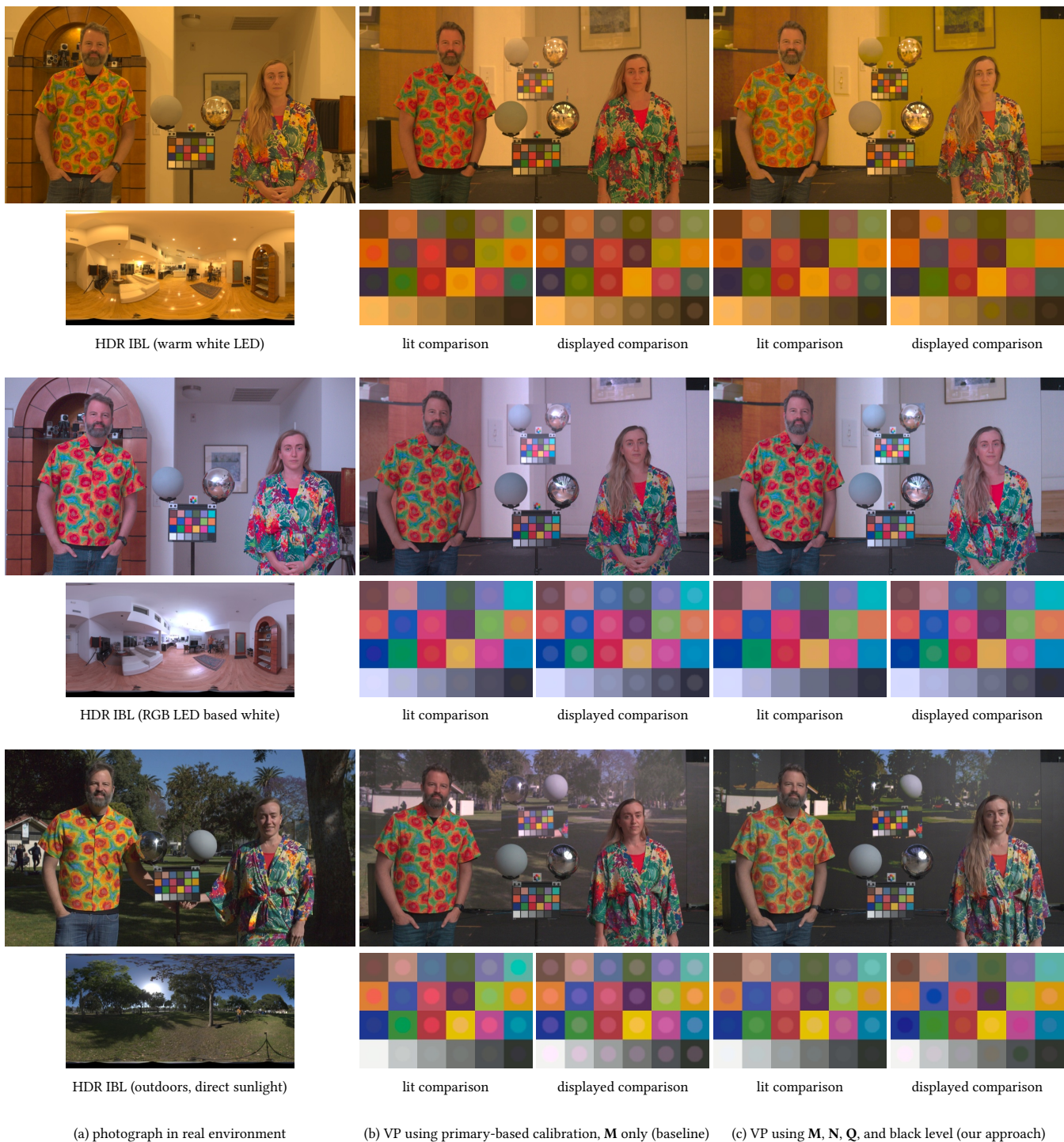


Figure 12: For three spectrally-diverse lighting environments, we show subjects photographed in the real world (a), lighting reproduction in a VP stage using the baseline approach (b), and using our full approach (c). Compared with the baseline calibration method, our approach enables improved color rendition for the *lit* chart, desaturating skin tones and improving the appearance of orange/yellow materials. Our black level subtraction removes the appearance of light bounced off the in-camera background LED panels. Observe the color rendition for the RGB LED based lighting environment (middle rows) is already quite good as we are asking RGB LED panels to reproduce RGB LED based illumination.

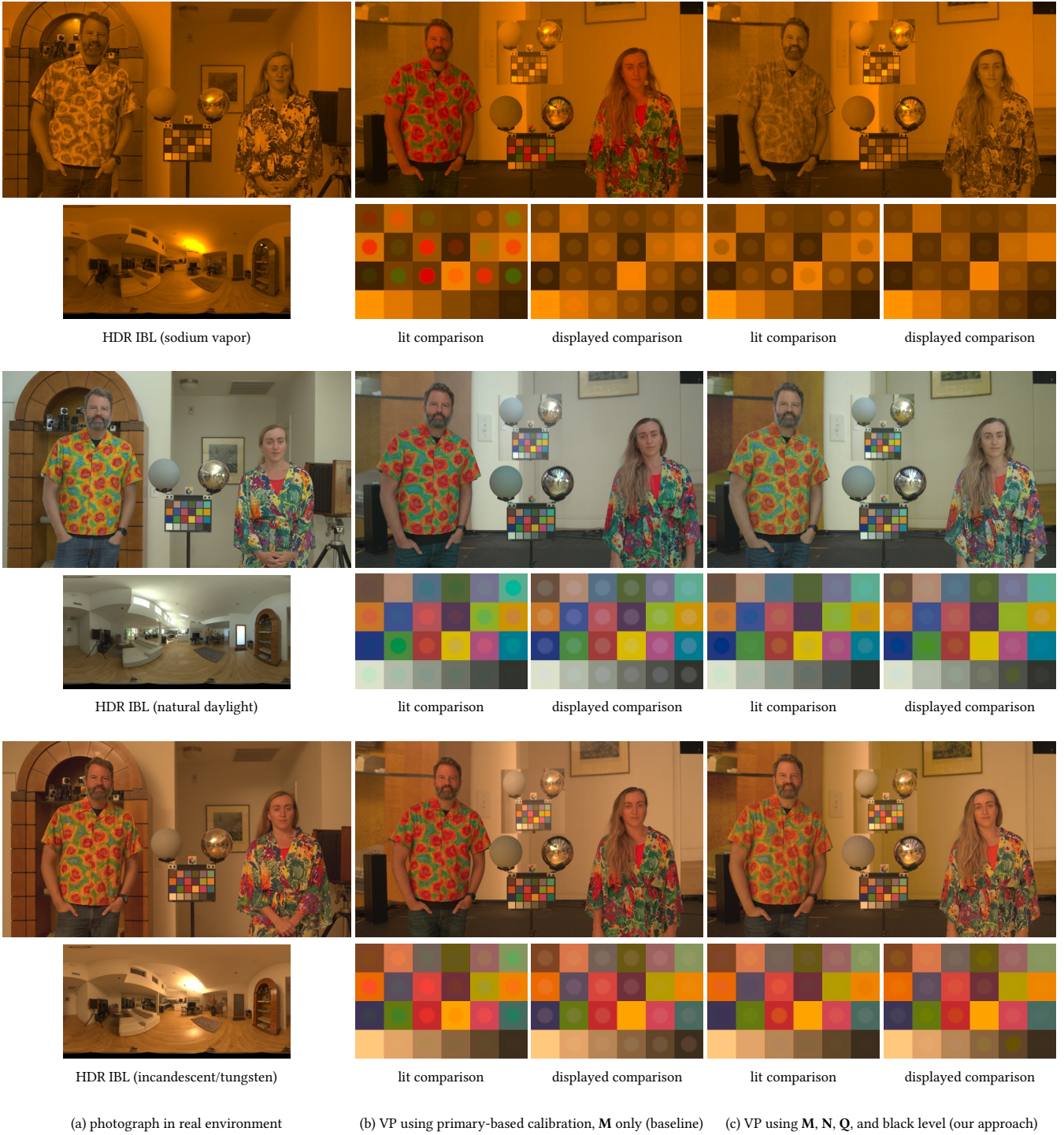


Figure 13: For three spectrally-diverse lighting environments, we show subjects photographed in the real world (a), lighting reproduction in a VP stage using the baseline approach (b), and using our full approach (c). Compared with the baseline calibration method, our approach enables improved color rendition for the *lit* chart, desaturating skin tones and improving the appearance of orange/yellow materials. Our black level subtraction removes the appearance of light bounced off the in-camera background LED panels. For the sodium vapor lighting environment of the top row, Q is able to completely desaturate the RGB-LED color chart in the VP stage to better match the appearance of the nearly monochromatic sodium vapor illumination in the real world.

despite our best attempts to calibrate the full system. As an example, see the results of Fig. 12 (bottom row). While we did our best to ensure panel linearity, we observed after our main experiments that the red LED channel exhibits its own single-channel non-linearity such that an image of the panel displaying a pixel value of $[0.5, 0, 0]$, multiplied by 2, does not equal an image of the panel displaying a pixel value of $[1, 0, 0]$. We suspect that a single-channel linearity calibration process involving a 3D lookup table (LUT) could mitigate this issue.

In Fig. 14 we show quantitative errors corresponding to the comparison color charts of Fig. 12 and Fig. 13. The solid bars represent the error for each color channel associated with the baseline approach, while the dashed bars represent error for our full approach. For both the out-of-frustum *lit* [Fig. 14(a)] and in-camera-frustum *displayed* [Fig. 14(b)] color charts, the average error relative to the white square intensity is under 4% for all lighting environments. The RGB LED lighting environment has the lowest average error, as expected, while the nearly monochromatic sodium vapor has the worst error for the *lit* color chart. These quantitative results are consistent with the visual observations from Fig. 12 and Fig. 13.

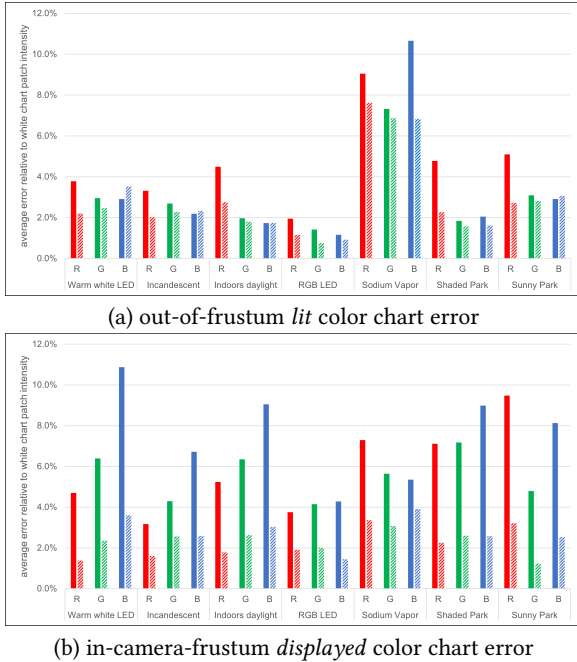


Figure 14: Average error relative to the white chart patch intensity value, for RGB channels individually and for each lighting environment, (a) for the out-of-frustum *lit* color chart, compared with the target color chart in the real world illumination, and (b) for the in-frustum *displayed* chart, also compared with the target. The solid bars represent error for the baseline approach (M only) while the dashed bars represent error for our full approach leveraging Q and, for the displayed chart, black level subtraction.

3.0.4 Theoretical Results. Although we have demonstrated the performance of our technique in practice, we also present theoretical results for the color chart lit by out-of-frustum content in the VP

stage, for each lighting environment. Rather than record the appearance of the color chart lit by the scene in the VP stage, as in the previous section, here we simulate the appearance of the color chart using Eqn. 3 and our calibration data, for the case using M only and then using M followed by the post-correction matrix Q . We show qualitative results in Fig. 15. As before, the color values sampled from a color chart illuminated in the real world form the background squares for each chart in the figure, while the foreground circles represent pixel values sampled from either the VP-produced method or the theoretical result. Our experimental results using Q [Fig. 15(d)] are very similar to the theoretical results using Q [Fig. 15(c)]. The remaining color error in [Fig. 15(d)], when our results are compared with the target color chart background squares, is therefore largely not the product of calibration or real-world system errors, but, rather, a fundamental limitation of using only 3×3 linear transformations to improve color rendition from RGB illumination.

4 FUTURE WORK

We have referred to our multi-matrix approach as *near optimal* rather than *optimal*, as we have first fixed the out-of-frustum matrix M and then subsequently solved for the post-correction matrix Q . Upon closer inspection, one could imagine minimizing the same objective function as in Eqn. 4, but jointly optimizing for M and Q simultaneously. Initially, we did try this joint optimization approach, but we found in practice that the resultant illumination in the VP stage appeared very non-neutral in color, and the post-correction matrix Q often had to make dramatic color adjustments. Beyond the obvious issue of such lighting being non ideal to actors immersed in the content of the VP stage, this optimization approach often led to out-of-gamut issues on the VP stage. Future work could explore this joint optimization approach, while constraining the white point of the content for better on set appearance and in-gamut content.

In our current approach, we have also not addressed the ideal color space of the content to be displayed. In our experiments, our HDRI maps were encoded in the camera raw of the Canon 5D Mark III camera, a relatively desaturated color space. This color space was somewhat sensible, as the majority of the displayed content was well within the achievable color gamut of the LED panels. However, a joint optimization approach could allow us to further reason about the ideal color space for the content to be displayed.

Additionally, the theoretical results of Fig. 15 demonstrate the limits of our proposed technique when leveraging 3×3 color matrix transforms. The lighting reproduced using RGB LEDs is fundamentally lacking energy in parts of the visible spectrum, so only so much color information can be recovered. Future work could leverage exemplar-based machine learning techniques to effectively hallucinate the appearance of materials under these missing parts of the EM spectrum based on multispectral image datasets or training data captured under both RGB and broad-spectrum illumination.

On typical virtual production sets, cinematographers may also wish to add practical light sources into the scene to enhance the look and feel of a particular shot. In our work, we have not yet addressed how to drive the LED panels and external practical lights *together* for optimal color rendition, which we view as an opportunity for

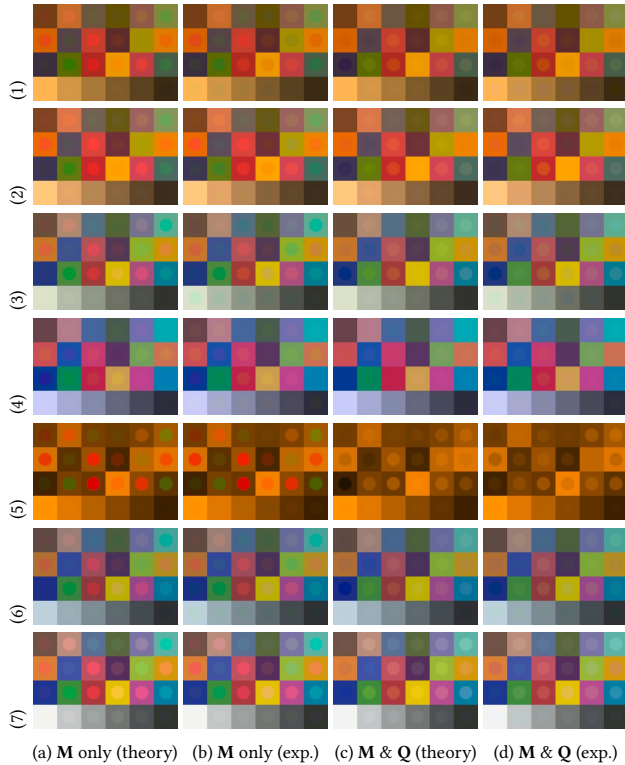


Figure 15: Comparison charts demonstrating the difference between our technique in theory and in experimental practice. Background squares are sampled from the chart in the real environment, while foreground circles are sampled from corresponding charts for each column label. (a) shows using M only for the *lit* chart, a theoretical result computed using Eqn. 3. (b) shows using M only, with pixel values sampled from images captured in the VP stage for the *lit* chart during our experiments. (c) shows adding Q to the theoretical result of (a). (d) shows adding Q to the experimental result of (b). Our experimental and theoretical results match closely. The lighting environments for each row are indicated at the left, using the labels of Fig. 10.

future work. We imagine that our current framework, however, may still be useful for this sub-problem.

Finally, although we have demonstrated the results of our technique using real-world photographed HDR IBL environments, our technique should apply as well when using rendered or computer-generated (CG) HDR IBL environments. However, one requirement of our technique is that we know the color rendition of the target lighting environment, provided via a color chart photographed in the original scene. One could either render such a color chart for a CG scene using a spectral rendering technique, or, alternatively if such a renderer is unavailable one could simply capture a photograph of a color chart in a similar real-world scene. For example, for a CG daylight environment, one could photograph a color chart in the real world in daylight as a record of the target color rendition. Future work could evaluate this proposed technique for bridging the

gap between rendered RGB HDR IBL environments and real-world measured color rendition.

5 CONCLUSION

We have presented a novel technique to improve the color rendition for RGB-LED based lighting reproduction, as applied towards today’s LED panel virtual production stages. In our approach, we treat the primary goal as improving the color rendition for materials illuminated by out-of-camera-frustum content in the LED volume, while treating in-camera color rendition as a secondary goal. Our technique requires only four calibration images: a record of how each LED appears to the motion picture camera and how each spectral channel of the RGB LED volume lights a color chart. We derive from these four images and a target color chart appearance three separate color transforms represented as 3×3 matrices: one that corrects in-frustum content, one that corrects out-of-frustum content, and one that is applied as a post-process to the acquired footage. We demonstrated that our method out-performs the previous state-of-the-art technique for color calibration, which only considers the in-camera background color appearance. Our technique is straightforward to practice, requiring only a few additional calibration images and straightforward shaders applied to a virtual production system.

ACKNOWLEDGMENTS

We thank Connie Siu and Stephan Trojansky for facilitating our VP stage capture session.

REFERENCES

- [n.d.]. In-camera VFX Camera Color Calibration. <https://docs.unrealengine.com/4.27/en-US/WorkingWithMedia/IntegratingMedia/InCameraVFX/InCameraVFXCameraCalibration/>
- [n.d.]. PTGui. <https://ptgui.com/>
- Paul Debevec. 1998. Rendering Synthetic Objects into Real Scenes: Bridging Traditional and Image-Based Graphics with Global Illumination and High Dynamic Range Photography. In *Proceedings of the 25th Annual Conference on Computer Graphics and Interactive Techniques (SIGGRAPH '98)*. Association for Computing Machinery, New York, NY, USA, 189–198. <https://doi.org/10.1145/280814.280864>
- Paul Debevec. 2003. HDRI and image-based lighting. *SIGGRAPH 2003 Course* (2003).
- Paul Debevec and Chloe LeGendre. 2022. HDR Lighting Dilation for Dynamic Range Reduction on Virtual Production Stages. (*arXiv.org*) (2022).
- Paul Debevec, Andreas Wenger, Chris Tchou, Andrew Gardner, Jamie Waese, and Tim Hawkins. 2002. A Lighting Reproduction Approach to Live-Action Compositing. *ACM Trans. Graph.* 21, 3 (Jul 2002), 547–556. <https://doi.org/10.1145/566654.566614>
- Pierre-Loïc Hamon, James Harmer, Stuart Penn, and Nicolas Scapel. 2014. Gravity: Motion Control and Face Integration. In *ACM SIGGRAPH 2014 Talks* (Vancouver, Canada) (*SIGGRAPH '14*). Association for Computing Machinery, New York, NY, USA, Article 35, 1 pages. <https://doi.org/10.1145/2614106.2614193>
- Jay Holben. 2020. The Mandalorian: This Is the Way. <https://ascmag.com/articles/the-mandalorian>
- Jack Holm, Tom Maier, Paul Debevec, Chloe LeGendre, Joshua Pines, Jonathan Erland, George Joblove, Scott Dyer, Blake Sloan, Joe di Gennaro, et al. 2016. A cinematographic spectral similarity index. In *SMPTE 2016 Annual Technical Conference and Exhibition*. SMPTE, 1–36.
- Noah Kadner. 2021a. 1899 Wraps Innovative Virtual Production. <https://ascmag.com/articles/1899-wraps-virtual-production>
- Noah Kadner. 2021b. Color Fidelity in LED Volumes. <https://ascmag.com/articles/color-fidelity-in-led-volumes>
- Noah Kadner. 2021c. On The Walls: Virtual Production for Series Shooting. <https://ascmag.com/articles/on-the-walls>
- Chloe LeGendre, Xueming Yu, and Paul Debevec. 2017. Optimal LED selection for multispectral lighting reproduction. *Electronic Imaging* 2017, 8 (2017), 25–32.
- Chloe LeGendre, Xueming Yu, Dai Liu, Jay Busch, Andrew Jones, Sumanta Pattanaik, and Paul Debevec. 2016. Practical Multispectral Lighting Reproduction. *ACM Trans. Graph.* 35, 4, Article 32 (Jul 2016), 11 pages. <https://doi.org/10.1145/2897824.2925934>

Andrea Weidlich, Alex Forsythe, Scott Dyer, Thomas Mansencal, Johannes Hanika, Alexander Wilkie, Luke Emrose, and Anders Langlands. 2021. Spectral imaging in production: course notes Siggraph 2021. In *ACM SIGGRAPH 2021 Courses*. 1–90.

Andreas Wenger, Tim Hawkins, and Paul Debevec. 2003. Optimizing color matching in a lighting reproduction system for complex subject and illuminant spectra. In *Rendering Techniques*. Citeseer, 249–259.